Estimates of Oxides of Nitrogen Formed in a Scramjet Inlet

L. M. Chiappetta* and J. J. Sangiovanni*
United Technologies Research Center, East Hartford, Connecticut 06108

Estimates of oxides of nitrogen formed in the inlet air stream were made for the forebody and internal sections of a generic inlet operating at high-speed flight conditions. Computational fluid dynamics analyses were used to compute typical inlet flow fields. Oxides of nitrogen levels were calculated using these flow fields together with a reaction rate mechanism as input to a chemical kinetics code. It was found that negligible amounts of these species are produced everywhere but in a small region of the air flow captured by the inlet and located near its surfaces. The static temperature reduction associated with oxides of nitrogen formation in the inlet is also insignificant except near inlet surfaces.

Introduction

STUDIES of propulsion systems for hypersonic flight involve consideration of the effects of chemical reactions in all sections of the engine. For most of the flight envelope, thrust is provided by means of a supersonic combustion ramjet (scramjet) engine. Different performance estimates are obtained depending on 1) whether the inlet air flow is in chemical equilibrium, chemically frozen, or in some intermediate state; 2) the amount of heat released in the combustor; and 3) the extent of recombination losses in the nozzle.

There is concern that scramjet performance is adversely affected by the formation of oxides of nitrogen in the inlet. For purposes of the present discussion, these compounds (NO, NO_2 and N_2O) are designated collectively as NO_x. The chemical reactions that produce NO_x are predominantly endothermic. Therefore, if NO_x production is significant, the temperature of the flow entering the combustor is decreased. While cooling the inlet flow can be beneficial since inlet flowrate can be increased, a performance penalty is incurred if the energy used to form NO_x is not recovered subsequently.

Scramjet performance estimates are often made using one-dimensional flow analyses. In some analyses, the flow is assumed to be in thermodynamic equilibrium. Thus, based on the average (one-dimensional) temperature at the exit of the inlet (entrance of the combustor), these analyses predict that significant amounts of NO_x are produced at high-speed flight conditions and that the combustor entrance temperature is decreased accordingly. If the combustor and nozzle flows are also assumed to be in equilibrium, then essentially all of this temperature decrease is recovered due, for example, to the effects of NO_x on hydrogen-air chemistry in equilibrium; in this case, the net effect of NO_x on scramjet performance is negligible. However, if either the combustor or the nozzle flow is not in thermodynamic equilibrium, then a performance decrement is predicted.

The question regarding the impact of NO_x formation on performance arises as a consequence of questions about the validity of the assumption of thermodynamic equilibrium. To examine this assumption, consider the processes that a fluid particle undergoes after it is captured by the inlet flow field. The typical scramjet inlet consists of a relatively long forebody followed by a relatively short internal section (see Fig. 1). The pressure and temperature of the fluid particle increase continuously from the free stream values to the values at the combustor entrance. The residence time for the typical fluid particle in the inlet flow field is of the order of a few milliseconds. Since the characteristic time for NO_x formation is also of the order of a few milliseconds, it is often argued that the flow at the combustor entrance is in thermodynamic equilibrium.

The amount of NO_x formed in the inlet air decreases in the combustor (due to decomposition caused by the high temperatures in the combustor) provided that the residence time in the combustor is long enough to achieve thermodynamic equilibrium. However, for high-speed flight, the residence time in the combustor is only a few microseconds. Therefore, only a negligible decrease of NO_x is likely to occur. NO_x formation and decomposition are very sensitive to temperature. Therefore, whatever NO_x exits the combustor is likely to persist in the nozzle since the static temperature in the nozzle decreases rapidly with distance. Nozzle recombination losses increase as NO_x concentration increases.

The present calculations were motivated by the knowledge that the production and decomposition of oxides of nitrogen are extremely sensitive to temperature. For constant temperature and pressure, the variation of NO_x concentration with time is shown in Fig. 2. Production of NO_x is generally negligible for temperatures below about 2000 K and NO_x decomposes rapidly at temperatures above about 3500 K. In addition, the molecular forms of oxygen (O_2) and nitrogen (N_2) dissociate significantly at temperatures above 2500 K and 4000 K, respectively. For still higher temperatures in excess of about 6000 K, ionization of NO, N, and O will occur.

The reaction mechanism for the formation of NO in high-temperature gas mixtures containing N_2 and O_2 was first proposed by Zeldovich, et al.[1] who suggested that

$$O + N_2 = NO + N \quad (1)$$

$$N + O_2 = NO + O \quad (2)$$

are the predominant reactions. Analytical studies by Duff and Davidson[2] on the chemistry of high temperature air have shown that these reactions are the major thermal sources of NO. This conclusion also has been verified experimentally, most notably by the work of Camac and Feinberg.[3] Both Reaction (1) and the reverse of Reaction (2) have been shown to have large activation energies which explains the strong temperature dependence of NO formation that has been observed experimentally. Moreover, because of this strong temperature dependence, the choice of rate constants used for Reactions (1) and (2) can have a significant effect on predictions of NO_x formation.

Presented as Paper 89-0197 at the AIAA 27th Aerospace Sciences Meeting, Reno, NV, Jan. 9–12, 1989; received March 30, 1989; revision received Oct. 12, 1990; accepted for publication Oct. 31, 1990.

*Senior Research Engineer.

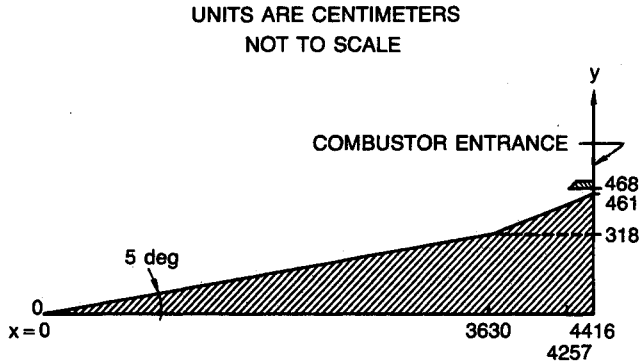

Fig. 1 Geometry for generic inlet.

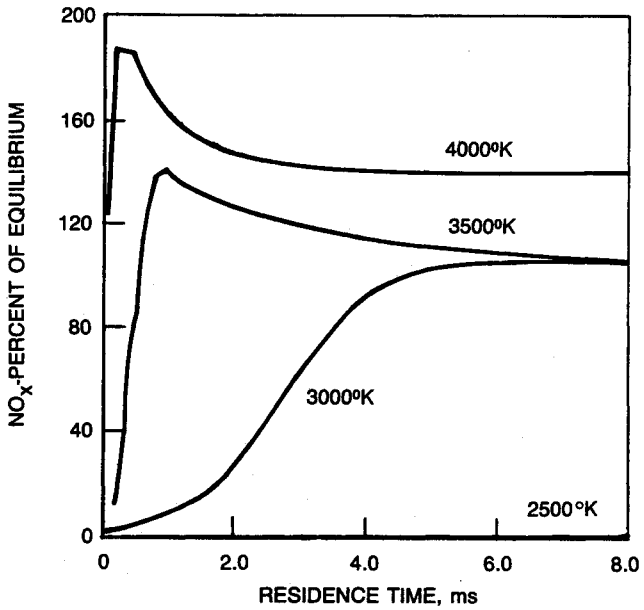

Fig. 2 Residence time effect on NO_x formation.

Since the identification of the "Zeldovich mechanism" in 1946, numerous research studies have been devoted to the evaluation of the rate constants for those reactions that contribute to the formation of NO_x in high temperature gas mixtures containing N_2 and O_2. The most reliable results of these studies have been included in comprehensive surveys of reaction rate data on NO_x formation, most notably by Baulch, et al.[4] and Hanson and Salimian.[5] Since the latter survey has considered the most recent research, and since it presents a consistent set of rate constants for the reactions that are known to contribute to NO_x formation, the reaction mechanism that was used for the present study was obtained from the survey by Hanson and Salimian. This mechanism, which is shown in Table 1, does not include the formation of ionized species because the inlet air static temperature is not expected to exceed 6000 K for sufficient time.

Approach

As noted above, production of NO_x is generally negligible below temperatures of 2000 K. Above a temperature of approximately 3500 K, NO_x decomposes. Strong temperature gradients exist throughout the inlet flow field. Necessarily, the surfaces of the inlet are cooled so that the temperature in the vicinity of the wall is probably 2000 K or less. As one proceeds outward from the surface, the static temperature first increases and then decreases. Thus, the region of NO_x formation is confined to only a portion of the flow field.

In order to determine the amount of NO_x formed in the inlet system without incurring the computational cost of solving the equations of motion together with the necessary species transport equations and chemical kinetic rates, a decoupled approach was used. Flow field calculations were performed using various assumptions noted below. These flow results were then used in a chemical kinetics computer program, together with the mechanism for N—O chemistry presented in Table 1, to determine the extent of chemical reaction.

Two inlet codes were used to compute the inlet flow field for the generic inlet design shown in Fig. 1 assuming various flight Mach numbers, the state of the boundary layer, and whether the flow was assumed to be chemically frozen or in chemical equilibrium. Input conditions are listed in Table 2.

Cases 1 and 2 provide a lower and an upper bound, respectively, for the inlet static temperature distribution since the formation of NO_x is endothermic. Cases 2 and 3 as well as Cases 4 and 5 provide a comparison of the effects of the boundary layer on NO_x formation. It should be noted that the computer codes used to obtain the flow fields do not contain detailed, chemical kinetics mechanisms. The effects of assuming that the flow is in equilibrium are confined to a table interpolation procedure used in the inlet flow field codes to determine the local static temperature. Cases 4 and 5 were included to permit investigation of the effects of lower free stream temperature.

The flow field calculation for the inlet forebody was obtained using the SCRAMP code and the flow field for the internal section of the inlet was computed using the SCRINT code. The 2D SCRAMP[6] and SCRINT[7] parabolized Navier-Stokes (PNS) codes are based on the 3D analysis of Schiff and Steger[8] using the upwind approach of Lawrence et al.[9] The PNS equations solved here are the full Navier-Stokes equations in which the time-dependent terms and all streamwise derivatives in the viscous flux terms have been neglected. The sublayer approximation described by Schiff and Steger is used to allow the PNS equations to be solved in a space-marching manner. The derivatives in the governing equations are represented by finite-difference approximations and the resulting nonlinear algebraic equation set is linearized about the downstream marching step, which results in an implicit algorithm. The SCRINT code is applied to internal flows by imposing no-slip, no-injection boundary conditions on both surfaces. The SCRAMP code is applied to external flow, where the leading edge shock is fitted at the upper boundary. The thermodynamics can be determined through perfect gas, equilibrium air, or frozen chemistry assumptions.

The flow field calculations were then interpolated to obtain flow conditions along several streamlines. Each streamline is designated by a number and represents the percentage of mass flow captured by the inlet that is confined between the inlet surface and that streamline. The streamlines were selected such that the streamline farthest from the body represents 99% of the flow captured by the internal section of the inlet. The streamlines are listed in Table 3. For the NO_x chemistry calculations described in this paper, Streamlines 1, 2, 4, 6, 8, 10, 12, 14, and 15 were used. Examples of the streamlines for Case 5 are shown in Fig. 3.

The variation of static temperature and static pressure along each streamline were used in conjunction with the CHEMKIN chemical kinetics code[10] to determine the changes in species composition. The CHEMKIN code computes the time variation of chemical species as a function of static pressure, static temperature, and initial composition. The chemical species considered included N, O, N_2, N_2O, NO, NO_2, and O_2. Thermodynamic properties for the constituents of air at high temperatures were obtained from the *JANAF Thermochemical Tables*.[11] For temperatures higher than 6000 K, thermodynamic properties were estimated using the methods of statistical mechanics, which are also described in Ref. 11. Note that the CHEMKIN code was used with the static temperature and pressure variations determined from the SCRAMP and SCRINT codes; the decrease in static temperature along the streamline due to the endothermic NO_x reactions was ignored.

Table 1 Chemical reaction mechanism for nitrogen-oxygen chemistry

Reaction cal/mol-K	k = A T^n exp(E/RT)		
	A	n	E (cal/mole)
$NO+M=N+O+M$	4.0E+20	−1.5	150000
$N_2O+M=N_2+O+M$	6.92E+23	−2.5	65000
$NO_2+M=NO+O+M$	1.10E+16	0.0	65570
$N_2+M=N+N+M$	3.72E+21	−1.6	224900
$O_2+M=O+O+M$	1.82E+18	−1.0	118000
$N_2+O=NO+N$	1.82E+14	0.0	76240
$NO+O=N+O_2$	3.80E+9	1.0	41370
$N_2O+O=NO+NO$	6.92E+13	0.0	26625
$N_2O+O=N_2+O_2$	1.00E+14	0.0	28020
$NO_2+O=NO+O_2$	1.00E+13	0.0	600
$NO_2+N=NO+NO$	4.00E+12	0.0	0
$NO_2+N=N_2O+O$	5.00E+12	0.0	0
$N_2O+N=N_2+NO$	1.00E+13	0.0	19900
$NO+N_2O=N_2+NO_2$	1.00E+14	0.0	49675
$NO_2+NO_2=NO+NO+O_2$	2.00E+12	0.0	26825

Table 2 Flow conditions

Case	Freestream conditions			Boundary[a] layer	Chemical state
	Mach number	Pressure, atm	Temperature, K		
1	25	1.1×10^{-3}	271	L/T	Equilibrium
2	25	1.1×10^{-3}	271	L/T	Frozen
3	25	1.1×10^{-4}	271	L	Frozen
4	12	4.6×10^{-3}	271	L	Frozen
5	12	4.6×10^{-3}	271	T	Frozen

[a]L = Laminar; T = Turbulent; L/T = Laminar-to-Turbulent transition included.

Table 3 Streamlines

No.	% Captured flow
1	1.0
2	2.0
3	3.0
4	4.0
5	5.0
6	10.0
7	20.0
8	30.0
9	40.0
10	50.0
11	60.0
12	70.0
13	80.0
14	90.0
15	99.0

Table 4 Static temperature reduction

Streamline	% Captured flow	Delta Ts (K)
1	1.0	0.2
2	2.0	—
4	4.0	—
6	10.0	—
8	30.0	—
10	50.0	—
12	70.0	—
14	90.0	0.5
15	99.0	211.0

Therefore, the results described below represent the maximum amounts of NO_x likely to be produced, especially at the conditions for Case 1.

Estimates of static temperature decrease due to the NO_x reactions were made by comparing the sensible enthalpy of the frozen flow at the exit of the inlet as provided by SCRINT and the sensible enthalpy from CHEMKIN at the last calculation station. A mean mixture heat capacity was used.

Results

For Case 1, the variation of static pressure and static temperature with residence time along Streamlines 1 and 15 are shown in Figs. 4 and 5, respectively. It is seen that fluid particles reach temperatures in excess of 2000 K for less than one millisecond. That is, the static temperature and static pressure along each streamline are lower than the values required for producing significant amounts of NO_x for most of the residence time of a fluid particle. Results for other streamlines and for other cases are similar. The rapid increase in static pressure or temperature within a relatively short distance (and time), as shown in these figures, is associated with the external shock system and the compression process occurring in the internal section of the inlet. For Case 1, the variation of residence time across the flow is essentially the same, varying for 5.4 to 5.6 ms. Similar results were obtained for the other cases. For Cases 1 through 3, static temperature profiles at the exit of the inlet (combustor entrance) are shown in Fig. 6. The static temperature is nearly uniform over the bulk of the flow. Significantly higher temperatures occur only near the inlet walls. Note that the results for Cases 1 and 2 justify the approach used in this study in which the flow field and chemical kinetics calculations are decoupled. The results for a fully coupled method can be expected to produce profiles intermediate to those obtained for Cases 1 and 2.

Results obtained for Case 1 using the CHEMKIN code are presented in Fig. 7 for NO, NO_2, and N_2O. The abscissa is the ratio of the mole fraction of the indicated species as determined by CHEMKIN to the equilibrium value based on the static temperature from SCRINT at the combustor entrance. The ordinate is the percent mass flow between each streamline and the lower surface of the inlet. Values of the abscissa greater than unity typically indicate that the equilib-

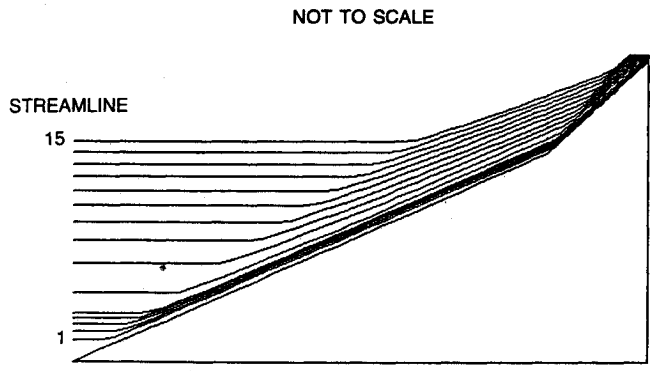

Fig. 3 Streamlines for Case 5.

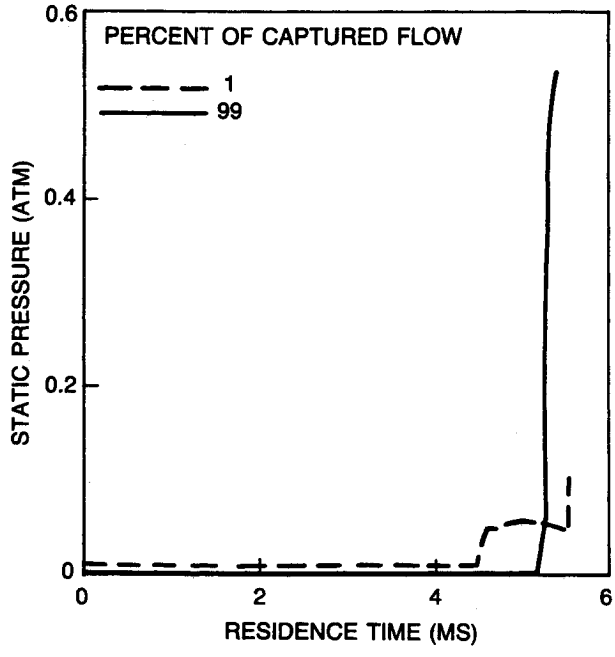

Fig. 4 Static pressure variation with flow residence time.

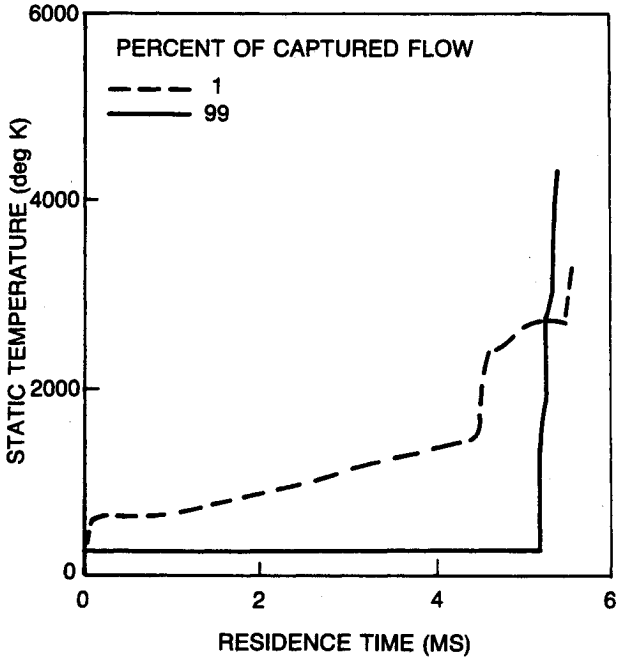

Fig. 5 Static temperature variation with flow residence time.

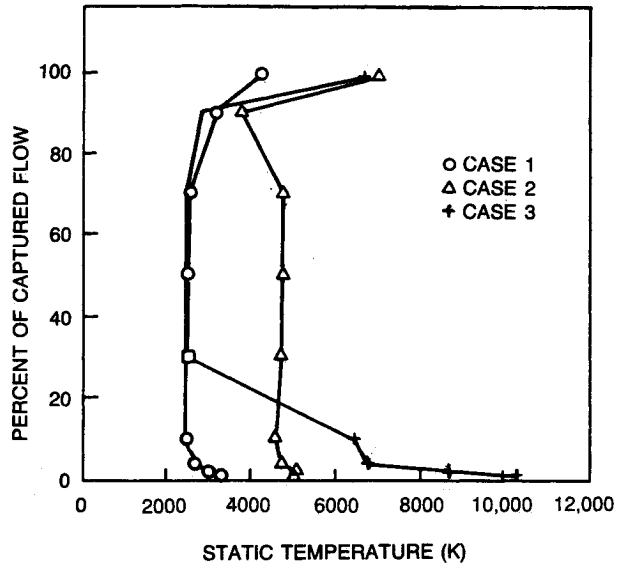

Fig. 6 Comparison of static temperature profiles at combustor entrance.

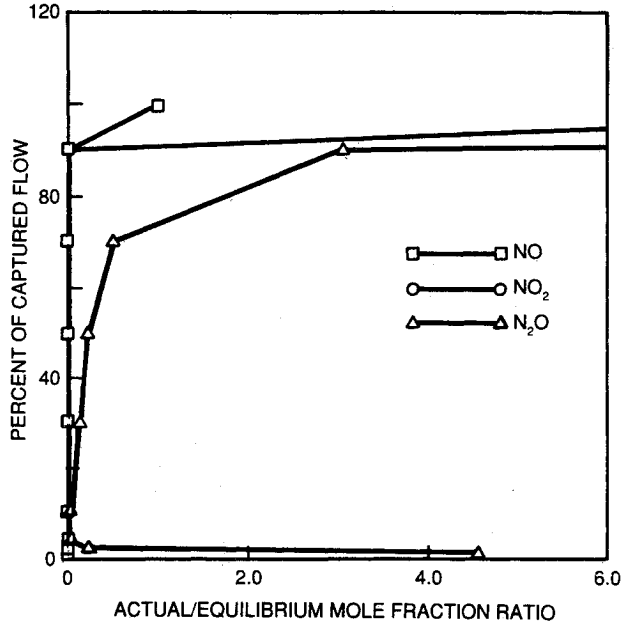

Fig. 7 Comparison of actual and equilibrium concentrations at combustor entrance.

rium value of a species is low. Results for N_2, O_2, N, and O are presented in tabular form in the Appendix. Except in the boundary layers, there is little dissociation of molecular nitrogen and oxygen. Thus, for most of the flow field, the ratio of actual to equilibrium mole fractions for both oxygen and nitrogen remain near unity.

Predicted mole fractions for all species at the combustor entrance for Cases 1 through 3 are presented in tabular form in the Appendix. For most of the flow, these results show that there is little difference in concentration levels due to the different assumptions made in computing the flow fields (see Table 2).

It is evident from these results that the concentrations of NO_x for the bulk of the flow are well below their equilibrium

values everywhere except in the boundary layers, i.e., large concentrations occur only near the walls. Note that at the highest temperatures, the large ratio of actual to equilibrium concentration is to some extent an indication of the small value of the denominator; that is, in equilibrium, a substantial portion of NO_x decomposes at high temperature. In any case, these results indicate that the assumption that the inlet flow is everywhere in equilibrium, even for the principal species, is poor; it may be more reasonable to assume that the flow is frozen. However, the present calculations were made to examine only the amount of NO_x produced in the inlet flow. It is possible that departure from either an equilibrium or a frozen chemistry assumption is more significant for other parameters of interest such as boundary layer results.

For the lower temperature cases (Cases 4 and 5), it was found that the amounts of NO_x produced anywhere in the flow field were much less than the levels found in Cases 1 through 3. Therefore, these results have been omitted. Results for an inlet operating both at Mach 10 and at Mach 13 have been reported by Yu, et al.[12] using a computer code in which the fluid mechanics and chemical kinetics equations are solved simultaneously. The chemical kinetics mechanism uses twenty-six reactions involving eleven species. Molar concentrations of various species are presented only along the bottom wall of the inlet. These results show that the flow is generally not in equilibrium, a result in agreement with those described herein.

For Case 1, the static temperature reduction due to NO_x chemistry at the exit of the inlet was also estimated, and is shown in Table 4; temperature reductions less than 0.1 K are omitted. Except for the outermost region of the flow (near the surface of the cowl), the temperature reduction is negligible. As noted earlier, both the amount of NO_x produced and the static temperature reduction are overestimated for this case.

Concluding Remarks

The results obtained using the flow fields computed by the inlet codes together with a chemical kinetics code indicate that the amounts of oxides of nitrogen produced at the high-speed flight condition are small and, perhaps, negligible. The corresponding static temperature reductions are also small except within a very small region of the flow. Consequently, there should be only minor effects of NO_x produced in the inlet on scramjet performance. That only small amounts of NO_x are produced is due to the fact that the static temperature along each streamline is in the range of maximum NO_x production for only a small fraction of the total residence time in the inlet.

It is known that NO_x reduces the ignition delay time for hydrogen-air chemical reactions.[13] However, for the high-speed flight regime, the static temperature in the combustor is high enough such that the effects of NO_x on ignition delay are negligible. For lower speed flight (e.g., Cases 4 and 5), the effects of NO_x are important, but the amount produced in the inlet is almost zero. The authors conclude that the effects of NO_x produced in the inlet on the chemistry in the combustor can be ignored.

Generally, for the inlet air flow, it is unnecessary to incur the computational cost of solving the equations of motion together with the necessary species transport equations and chemical kinetic rates. However, the possibility exists that accurate calculation of some of the boundary layer parameters may require an analysis that includes the effects of finite-rate chemistry. However, in this case it may be possible to develop a simplified reaction mechanism using only one or two chemical reactions; i.e., a global heat absorption mechanism may be adequate to obtain the correct static pressure and static temperature distributions. In any case, the assumption that the inlet air flow is in thermodynamic equilibrium cannot be justified.

Appendix: Composition Of Air At Combustor Inlet

Concentrations are indicated by actual and equilibrium mole fractions, an asterisk (*) indicates that species were not computed because concentrations are very small; less than 1.0E−06.

Case 1

Streamline		1	2	4	6	8	10	12	14	15
Temperature (K)		3270	2970	2660	2470	2500	2480	2560	3130	4230
Pressure (atm)		0.102	0.149	0.207	0.321	0.485	0.505	0.518	0.521	0.531
N:	Actual	0.990E−08	0.115E−09	0.277E−11	0.197E−11	0.170E−10	0.245E−10	0.127E−09	0.214E−07	0.793E−04
	Equil.	0.178E−03	0.253E−04	0.225E−05	0.341E−06	0.368E−06	0.285E−06	0.611E−06	0.365E−04	0.432E−02
O:	Actual	0.274E−04	0.103E−05	0.986E−07	0.115E−06	0.772E−06	0.127E−05	0.442E−05	0.811E−04	0.214E−01
	Equil.	0.210E+00	0.959E−01	0.280E−01	0.961E−02	0.907E−02	0.788E−02	0.116E−01	0.874E−01	0.307E+00
N_2:	Actual	0.790E+00	0.790E+00	0.790E+00	0.790E+00	0.790E+00	0.790E+00	0.790E+00	0.790E+00	0.767E+00
	Equil.	0.689E+00	0.734E+00	0.765E+00	0.775E+00	0.775E+00	0.776E+00	0.773E+00	0.733E+00	0.651E+00
N_2O:	Actual	0.244E−05	0.157E−06	0.156E−07	0.183E−07	0.111E−06	0.167E−06	0.451E−06	0.483E−05	0.619E−04
	Equil.	0.536E−06	0.697E−06	0.640E−06	0.612E−06	0.792E−06	0.776E−06	0.898E−06	0.159E−05	0.100E−05
NO:	Actual	0.427E−06	0.558E−09	0.101E−10	0.252E−10	0.106E−08	0.307E−08	0.279E−07	0.298E−05	0.280E−01
	Equil.	0.348E−01	0.368E−01	0.284E−01	0.218E−01	0.229E−01	0.220E−01	0.252E−01	0.445E−01	0.277E−01
NO_2:	Actual	0.391E−09	0.789E−13	0.543E−15	0.323E−14	0.622E−12	0.285E−11	0.374E−10	0.308E−08	0.133E−04
	Equil.	0.263E−05	0.594E−05	0.819E−05	0.989E−05	0.124E−04	0.125E−04	0.131E−04	0.120E−04	0.115E−05
O_2:	Actual	0.210E+00	0.210E+00	0.210E+00	0.210E+00	0.210E+00	0.210E+00	0.210E+00	0.210E+00	0.183E+00
	Equil.	0.653E−01	0.134E+00	0.179E+00	0.193E+00	0.193E+00	0.194E+00	0.190E+00	0.135E+00	0.989E−02

Case 2

Streamline		1	2	4	6	8	10	12	14	15
Temperature (K)		5020	5090	4710	4600	4740	4750	4770	3750	7070
Pressure (atm)		0.215	0.281	0.356	0.619	0.988	1.02	0.994	0.549	0.535
N:	Actual	0.396E−04	0.150E−04	0.371E−05	0.444E−05	0.130E−04	0.114E−04	0.128E−04	0.184E−05	0.129E+00
	Equil.	0.575E−01	0.590E−01	0.213E−01	0.121E−01	0.139E−01	0.141E−01	0.150E−01	0.739E−03	0.580E+00
O:	Actual	0.404E−02	0.161E−02	0.663E−03	0.850E−03	0.194E−02	0.171E−02	0.185E−02	0.136E−02	0.299E+00
	Equil.	0.329E+00	0.328E+00	0.329E+00	0.321E+00	0.319E+00	0.319E+00	0.320E+00	0.243E+00	0.245E+00
N_2:	Actual	0.788E+00	0.789E+00	0.790E+00	0.790E+00	0.789E+00	0.789E+00	0.789E+00	0.789E+00	0.543E+00
	Equil.	0.597E+00	0.596E+00	0.634E+00	0.643E+00	0.640E+00	0.640E+00	0.639E+00	0.672E+00	0.168E+00
N_2O:	Actual	0.283E−03	0.183E−03	0.814E−04	0.906E−04	0.157E−03	0.149E−03	0.157E−03	0.352E−04	0.846E−05
	Equil.	0.202E−06	0.266E−06	0.441E−06	0.836E−06	0.117E−05	0.119E−05	0.115E−05	0.152E−05	*
NO:	Actual	0.824E−03	0.126E−03	0.277E−04	0.508E−04	0.240E−03	0.184E−03	0.214E−03	0.303E−03	0.283E−01
	Equil.	0.843E−02	0.908E−02	0.146E−01	0.210E−01	0.231E−01	0.232E−01	0.226E−01	0.419E−01	0.163E−02
NO_2:	Actual	0.337E−06	0.485E−07	0.113E−07	0.225E−07	0.106E−06	0.806E−07	0.932E−07	0.214E−06	0.124E−06
	Equil.	0.392E−07	0.587E−07	0.175E−06	0.518E−06	0.706E−06	0.721E−06	0.662E−06	0.449E−05	*
O_2:	Actual	0.207E+00	0.209E+00	0.210E+00	0.209E+00	0.209E+00	0.209E+00	0.209E+00	0.209E+00	0.164E−02
	Equil.	0.457E−03	0.501E−03	0.170E−02	0.388E−02	0.410E−02	0.411E−02	0.381E−02	0.418E−01	0.188E−04

Case 3

Streamline		1	2	4	6	8	10	12	14	15
Temperature (K)		10300	8700	6770	6430	2420	2460	2480	2840	6680
Pressure (atm)		0.0995	0.104	0.106	0.0447	0.0334	0.0424	0.0478	0.0506	0.0513
N:	Actual	0.944E−01	0.138E−01	0.595E−03	0.272E−04	0.434E−11	0.972E−11	0.122E−10	0.321E−10	0.756E−04
	Equil.	0.784E+00	0.782E+00	0.669E+00	0.663E+00	0.650E−06	0.850E−06	0.968E−06	0.177E−04	0.706E+00
O:	Actual	0.183E+00	0.857E−01	0.149E−01	0.161E−02	0.253E−06	0.528E−06	0.617E−06	0.540E−06	0.312E−02
	Equil.	0.211E+00	0.211E+00	0.230E+00	0.231E+00	0.226E−01	0.246E−01	0.255E−01	0.102E+00	0.224E+00
N_2:	Actual	0.560E+00	0.687E+00	0.780E+00	0.789E+00	0.790E+00	0.790E+00	0.790E+00	0.790E+00	0.788E+00
	Equil.	0.230E−03	0.229E−02	0.948E−01	0.100E+00	0.771E+00	0.770E+00	0.769E+00	0.734E+00	0.648E−01
N_2O:	Actual	0.103E−02	0.354E−02	0.180E−02	0.314E−03	0.412E−07	0.835E−07	0.963E−07	0.864E−07	0.582E−03
	Equil.	*	*	*	*	0.176E−06	0.212E−06	0.233E−06	0.341E−06	*
NO:	Actual	0.144E+00	0.109E+00	0.477E−02	0.516E−04	0.931E−10	0.390E−09	0.565E−09	0.328E−09	0.195E−03
	Equil.	0.864E−05	0.410E−04	0.584E−03	0.463E−03	0.195E−01	0.208E−01	0.215E−01	0.311E−01	0.341E−03
NO_2:	Actual	0.648E−05	0.226E−04	0.172E−05	0.160E−07	0.160E−13	0.122E−12	0.222E−12	0.937E−13	0.642E−07
	Equil.	*	*	*	*	0.297E−05	0.340E−05	0.364E−05	0.324E−05	*
O_2:	Actual	0.169E−01	0.101E+00	0.198E+00	0.209E+00	0.210E+00	0.210E+00	0.210E+00	0.210E+00	0.208E+00
	Equil.	0.161E−06	0.516E−06	0.488E−05	0.339E−05	0.187E+00	0.185E+00	0.184E+00	0.133E+00	0.253E−05

References

[1]Zeldovich, Ya. B., Sadovnikov, P. Ya., and Frank-Kamenetskii, D. A., "Oxidation of Nitrogen in Combustion," (M. Shelef, Translator), Academy of Science USSR, Institute Chemistry and Physics, Moscow-Leningrad, USSR, 1947.

[2]Duff, R. E., and Davidson, N., *Journal Chemistry Physics*, 31, 1959, pp. 1018–1027.

[3]Camac, M., and Feinberg, R. M., Eleventh Symposium (International) on Combustion, The Combustion Institute, Pittsburgh, PA, 1967, pp. 137–145.

[4]Baulch, D. L., Drysdale, D. D., and Horne, D. G., *Evaluated Kinetic Data for High Temperature Reactions*, Vols. 2 and 3, Butterworths, London, England, 1973 and 1976.

[5]Hanson, R. K., and Salimian, S., "Survey of Rate Constants in the N/H/O System." *Combustion Chemistry*, edited by W. C. Gardiner, Jr., Springer-Verlag, New York, NY, 1984, pp. 361–421.

[6]Krawczyk, W. J., Rajendran, N., Harris, T. B., York, B. J., and Dash, S. N., "Computational Models for the Analysis/Design of Hypersonic Scramjet Components—Part II, Inlet and Ramp/Forebody Models," AIAA/ASME/SAE/ASEE 22nd Joint Propulsion Conference, Paper No. 86-1596, Huntsville, AL, June 16–18, 1986.

[7]Krawczyk, W. J., and Harris, T. B., "Parabolized Navier-Stokes Analysis of Two-Dimensional Scramjet Inlet Flow Fields," AIAA Paper 87-1899, June 1987.

[8]Schiff, L. B., and Steger, J. L., "Numerical Simulation of Steady Supersonic Viscous Flows," NASA TP-1749, 1981.

[9]Lawrence, S. L., Tannehill, J. C., and Chaussee, D. S., "An Upwind Algorithm for the Parabolized Navier-Stokes Equations," AIAA Paper 86-1117, May 1986.

[10]Kee, R. J., Miller, J. A., and Jefferson, T. H., "CHEMKIN—A General Purpose, Problem Independent Transportable Fortran Chemical Kinetics Code Package," Sandia National Laboratory, Albuequerque, NM, Report SAND80-8003, March 1980.

[11]Stull, D. R., and Prophet, H., et al., "JANAF Thermochemical Tables," Second Edition, U.S. Department of Commerce, National Bureau of Standards, NSRDS-NBS37, June 1971.

[12]Yu, S., McBride, B. J., Hsieh, K., and Shuen, J., "Numerical Simulation of Hypersonic Inlet Flows with Equilibrium and Finite Rate Chemistry," AIAA 26th Aerospace Sciences Meeting, Paper No. 88-0273, Reno, NV, January 11–14, 1988.

[13]Slack, M., and Grillo, A., "Investigation of Hydrogen-Air Ignition Sensitized by Nitric Oxide and by Nitrogen Dioxide," NASA CR-2896, October 1977.